Electron beam probing of non-equilibrium carrier dynamics in 18 MeV alpha particle- and 10 MeV proton-irradiated Si-doped β-Ga_2O_3 Schottky rectifiers

Sushrut Modak [a)], Leonid Chernyak [a,h)] , Minghan Xian [b)], Fan Ren [b)],

Stephen J. Pearton [c)], Igor Lubomirsky [d)], Arie Ruzin [e)], Vladimir P. Drachev [f,g)]

[a] *Department of Physics, University of Central Florida, Orlando, FL 32816, USA*

[b] *Department of Chemical Engineering, University of Florida, Gainesville, FL 32611, USA*

[c] *Material Science and Engineering, University of Florida, Gainesville, FL 32611, USA*

[d] *Department of Materials and Interfaces, Weizmann Institute of Science, Rehovot 76100, Israel*

[e] *School of Electrical Engineering, Tel Aviv University, Tel Aviv 69978, Israel*

[f] *Skolkovo Innovation Ctr, Skolkovo Inst Sci & Technol, Ctr Photon & Quantum Mat, Nobel St, Bldg 3, Moscow 121205, Russia*

[g] *Univ North Texas, Dept Phys, Denton, TX 76203 USA*

Minority hole diffusion length and lifetime were measured in independent experiments by Electron Beam-Induced Current and Time-Resolved Cathodoluminescence in Si-doped β-Ga_2O_3 Schottky rectifiers irradiated with 18 MeV alpha particles and 10 MeV protons. Both diffusion length and lifetime were reduced with increasing temperature. Non-equilibrium minority hole mobility was calculated based on the independently measured diffusion length and lifetime, indicating that the so-called "hole self-trapping" is most likely irrelevant in the 77-295 K temperature range.

[h)] email: chernyak@physics.ucf.edu

β-Ga_2O_3 is a group-III semiconductor oxide with a bandgap of ~ 4.7 eV. Over the past decade, it has become increasingly attractive due to its robustness and applications in high-power electronics, optoelectronic devices in ultraviolet (UV) regime, true solar-blind UV detection and as a transparent conductive substrate [1-6]. Over the last decade, minority carrier transport properties such as diffusion length, lifetime and mobility in n-type β-Ga_2O_3 were extensively studied [7-10]. The realization of p-type conductivity remains a challenge because of the self-trapped nature of holes, leading to low mobility ($1x10^{-6}$ $cm^2V^{-1}s^{-1}$) [10]. Contrary to this prediction, the relatively high experimental values for hole diffusion length in n-type β-Ga_2O_3 (50-600 nm) indicate that holes were indeed mobile at room-temperature and their self-trapped nature is likely relevant for temperatures below 120 K [9, 11].

A limited number of techniques are available to directly determine the mobility of excess non-equilibrium carriers. Recently, the pump-probe technique was used to measure the dynamics of self-trapped holes [12] and self-trapped excitons [13]. Moreover, lifetimes of ~ 200 ps for conduction electrons resulted from fast light pulse excitation [14]. Lee *et al.* measured diffusion length (L) and excess carrier lifetime (τ) independently in Si-doped β-Ga_2O_3 Schottky rectifiers subjected to 1.5 MeV electron irradiation [9] using Electron Beam-Induced Current (EBIC) and Time-Resolved Cathodoluminescence (TRCL). At room temperature, L and τ were found to be 330 nm and 215 ps respectively, resulting in a surprisingly high non-equilibrium hole mobility (μ) of ~ 200 $cm^2V^{-1}s^{-1}$. These values were found to reduce significantly with exposure to electron irradiation with varying fluences.

Experimental measurements of L, τ and μ for excess non-equilibrium holes in n-type β-Ga_2O_3 exposed to various radiation sources, and their temperature dependence, are desirable. In this study, the focus is on measurement of minority transport properties, namely L and τ, in Si-

doped β-Ga_2O_3 Schottky rectifiers, exposed to proton and alpha-particle radiation in the temperature range 77-295 K.

Sn-doped (n^+, carrier concentration ~ 2.2×10^{18} cm^{-3}) β-Ga_2O_3 substrates (orientation [001]) grown by Edge-Defined Film-Fed Growth (EFG) technique were used for deposition of epitaxial β-Ga_2O_3 layers with Halide Vapor Phase Epitaxy (HVPE). The 20 μm thick epitaxial layer was doped with Si (electron concentration ~ 3.6×10^{16} cm^{-3}) and was planarized to a thickness of 10 μm with chemical/mechanical polishing. Schottky contacts were fabricated by Ni/Au deposition (20 nm/80 nm) on the epitaxial layer, followed by photolithography and liftoff. Finally, Ohmic contacts on the backside of the substrate were made by blanket deposition of Ti/Au (20 nm/80 nm). A schematic diagram of the rectifiers is shown in Fig. 1a. The samples were divided in groups, with the first as controls. The second group was exposed to 10 MeV proton radiation generated by MC-50 cyclotron at Korea Institute of Radiological and Medical Science with a fluence of $5x10^{14}$ cm^{-2}. The proton beam completely irradiated the epitaxial β-Ga_2O_3 layer with a range of 330 μm in the material. Similarly, the third group of samples was exposed to 18 MeV alpha particle radiation with a fluence of $1x10^{12}$ cm^{-2} and penetration depth of 80 μm. The beam current of the cyclotron was 100 nA in both cases. Furthermore, the carrier removal rates of the proton- and alpha particle-irradiated samples were measured to be 237 cm^{-1} and 406 cm^{-1}, respectively. Additional irradiation and fabrication details can be found elsewhere [15, 16].

L and τ were measured *in-situ* in Attolight Chronos Scanning Electron Microscope (SEM) fitted with a temperature-controlled stage (CryoVAC TIC 500) using EBIC line-scan technique (planar configuration) and TRCL, respectively. Beam energy was kept fixed at 10 keV for both techniques with electron range (R_e) of 0.4 μm in the material [17]. The ratio $R_e/L < 4$ ensured L not to be limited by EBIC resolution [18]. The EBIC signal was amplified with Stanford Research

Systems low-noise amplifier (SR570) and recorded with Keithley DMM 2000 digital multimeter connected to a PC with data acquisition software. Fig. 1b shows an EBIC line-scan acquired at 77 K. The cathodoluminescence (CL) signal was collected by a mirror assembly directly above the sample. This assembly is spatially coupled to a streak camera (Optronis Optoscope) with a minimum resolution ~ 2 ps. The time-resolved mode of operation was achieved with generation of electron pulses with ~ 8 ps width by focusing a femtosecond laser (Onefive Genki HP-03, 80 MHz), synchronized with the streak camera, on electron gun tip.

L was extracted from the EBIC line-scan according to [19, 20]:

$$I_{EBIC}(x) = I_0 x^{\alpha} \exp\left(-\frac{x}{L}\right). \quad (1)$$

Here, I_0 is a constant; x is the distance from the junction to the electron beam; L is the minority hole diffusion length; and α is a constant related to surface recombination velocity. Furthermore, α = -0.5, indicating a low influence of surface recombination velocity, was chosen for analysis. A fit to EBIC signal acquired at 77 K with $x^{\alpha}exp(-x/L)$ is shown in Fig. 1b (inset). A strong correlation between the beam probe current and L was discovered (with a different location for every measurement), indicating the sensitivity of the material to electron beam exposure. The dependence of L on extended duration electron beam exposure in β-Ga_2O_3 and other wide band gap semiconductors was reported in earlier studies, where the final value of L depends on the net charge density deposited in the region of the measurement [7, 21-28]. The rate of L enhancement with the net deposited charge in alpha- and proton-irradiated structures was found to be lower compared to the control sample [22]. In this study, a new location is chosen for every EBIC line-scan along with a small beam current of ~ 8 pA, to minimize the charge injection effect.

The temperature dependence of L for control, alpha- and proton-irradiated diodes is shown in Fig. 2. Activation energy for the temperature dependence of L can be extracted from [25, 29]:

$$L(T) = L_0 \exp\left(\frac{\Delta E_{A,T}}{2kT}\right). \quad (2)$$

Here, L_0 is a constant; $\Delta E_{A,T}$ is thermal activation energy; k is the Boltzmann constant; and T is the temperature in Kelvin. $\Delta E_{A,T}$ for control, alpha- and proton-irradiated structures were calculated as 5.4, 4.1 and 3.7 meV indicating a weak temperature dependence. In earlier studies on ZnO, GaN and Ga_2O_3 [20, 21, 25, 26], $\Delta E_{A,T}$ was associated with trap levels in the forbidden gap, but the currently obtained values are clearly smaller than activation energies of any known trap levels in the bandgap. A probable origin of the activation energy is the increased carrier recombination with rise in the temperature. A direct factor contributing to the low activation energy is the relatively small value of L compared to other reported values, likely originating from the charge injection effect due to the magnitude of the electron beam current in use [8, 9, 16].

A TRCL streak of the characteristic ultraviolet luminescence (UVL) centered around 380 nm in β-Ga_2O_3 is shown in Fig. 3 (continuous CL spectra are given in ref. [9]) [30]. The TRCL streak from Fig. 3 follows a single exponent decay described by:

$$A(t) = A_0 \exp(-t/\tau) + C. \quad (3)$$

Here, A_0 is the initial integrated CL intensity; t is the delay after excitation; τ is the decay constant and C is a constant associated with luminescence persisting longer than the excitation period of 12.5 ns (80 MHz). Eq. (3) is consistent with observation of fast and slow decay constants by Binet and Gourier [31]. In this study, for the picosecond measurement timescale, C is approximated as a constant during the extraction of lifetime. τ is obtained by fitting the streak signal with Eq. (3) [9, 32].

In this research, τ decreased from 572 ps, 523 ps and 464 ps at 77 K to 168 ps, 159 ps and 154 ps at 295 K for control, alpha- and proton-irradiated samples, respectively (Fig. 4). The irradiated structures sustain additional point defects due to radiation damage and, therefore, exhibit reduction in L as well as τ. The values of L and τ were largest for the control structure, followed by alpha- and lastly, by proton-irradiated structures. This could be attributed to the fluence of proton irradiation being over two orders of magnitude larger than alpha-irradiation.

UVL in Si-doped β-Ga_2O_3 is associated with the self-trapped excitons (STEs) and recombination involving Si_{Ga} donors and V_{Ga}, V_O-V_{Ga} complexes [33]. Onuma *et al.* discovered that around 150 K, where most STEs have thermally disassociated, non-radiative recombination centers (NRCs) play a significant role in carrier recombination. This was expressed in Si-doped β-Ga_2O_3 by CL thermal quenching with increasing temperature [34]. A recent study by Huynh *et al.* of UVL in β-Ga_2O_3 identified the presence of Fe^{3+} impurity (~ 0.6 eV below conduction band minimum), that acts as an efficient non-radiative recombination center, inhibiting the carriers from participation in other recombination channels [35]. Saturation of Fe^{3+} centers, facilitating non-radiative recombination, was studied by observing the CL signal magnitude with variation of the electron beam current. At temperatures above 150 K, ionization of Si-donors, emission of weakly bound electrons from STEs (increases the number of available recombination centers) [32, 34], and participation of NRCs, are likely responsible for reduction in excess carrier lifetime with increasing temperature in Fig. 4.

In this research, under low injection conditions (beam current of 8 pA), the excess carrier lifetime from a mono-exponential TRCL decay is assumed to be equal to the minority carrier lifetime (hole lifetime, in this case) [36, 37]. The minority carrier diffusion length and lifetime are related by the Einstein relation:

$$L = \sqrt{D\tau} = \sqrt{\mu k_B T \tau / q}. \quad (4)$$

Here, D is the diffusivity; and q is the electron charge. Eq. (4) contains L and τ measured from independent experiments and can be used to calculate minority carrier mobility (μ). Fig. 5 shows variation of μ with temperature for control, alpha and proton irradiated samples. It is worth mentioning that τ, used in Eq. (4) for mobility calculations, is obtained under short (~ 8 picosecond) laser excitation pulses. Therefore, the calculated mobility is transient in nature and is different from Hall mobility varying with temperature as $T^{\pm 3/2}$. While room temperature mobility calculated in ref. [9], following a similar approach, was in excess of ~ 200 $cm^2V^{-1}s^{-1}$ for L = 330 nm and τ = 215 ps in a control sample, room temperature μ found in this study was ~25 $cm^2V^{-1}s^{-1}$ for L = 106 nm and τ = 168 ps. This indicates L impact on calculated transient mobility for non-equilibrium minority holes. The latter mobility is two-to-three orders of magnitude higher than the measured equilibrium majority hole mobility of 0.2 $cm^2V^{-1}s^{-1}$ in p-type β-Ga_2O_3 [38].

In this study, the activation energies of ≤ 5.5 meV, pertaining to a decrease of L with increasing temperature, likely originate from the increase in the carrier recombination rate. This is confirmed by simultaneous reduction in the lifetime. L measured in this study is not impacted by charge injection effects and is, therefore, lower compared to the previously reported values [7, 9]. Alpha- and proton-irradiation introduced additional recombination centers that resulted in reduction of L and τ. Further, the activation energy extracted from the temperature dependence of L, decreased for the irradiated structures, thereby reducing the thermal barrier for carrier recombination.

The research at UCF and the Weizmann Institute was supported in part by NATO (award # G5453) and NSF (UCF award # ECCS1802208). Research at UCF and Tel Aviv University was supported in part by US-Israel BSF (2018010). The work at UF was performed as part of the Interaction of Ionizing Radiation with Matter University Research Alliance (IIRM-URA), sponsored by the Department of the Defense, Defense Threat Reduction Agency under award HDTRA1-20-2-0002, monitored by Jacob Calkins and also by NSF DMR 1856662 (J.H. Edgar).

References

1. S.J. Pearton, J. Yang, P.H. Cary, F. Ren, J. Kim, M.J. Tadjer, and M.A. Mastro, Appl. Phys. Rev. **5**, 011301 (2018).
2. J.Y. Tsao, S. Chowdhury, M.A. Hollis, D. Jena, N.M. Johnson, K.A. Jones, R.J. Kaplar, S. Rajan, C.G. Van de Walle, E. Bellotti, C.L. Chua, R. Collazo, M.E. Coltrin, J.A. Cooper, K.R. Evans, S. Graham, T.A. Grotjohn, E.R. Heller, M. Higashiwaki, M.S. Islam, P.W. Juodawlkis, M.A. Khan, A.D. Koehler, J.H. Leach, U.K. Mishra, R.J. Nemanich, R.C.N. Pilawa-Podgurski, J.B. Shealy, Z. Sitar, M.J. Tadjer, A.F. Witulski, M. Wraback, and J.A. Simmons, Adv. Electron. Mater. **4**, 1600501 (2018).
3. H. von Wenckstern, Adv. Electron. Mater. **3**, 1600350 (2017).
4. M. Kim, J.-H. Seo, U. Singisetti, and Z. Ma, J. Mater. Chem. C **5**, 8338-8354 (2017).
5. M. Higashiwaki, K. Sasaki, H. Murakami, Y. Kumagai, A. Koukitu, A. Kuramata, T. Masui, and S. Yamakoshi, Semicond. Sci. Technol. **31**, 11 (2016).
6. K. Akito, K. Kimiyoshi, W. Shinya, Y. Yu, M. Takekazu, and Y. Shigenobu, Jpn. J. Appl. Phys. **55**, 1202A2 (2016).
7. S. Modak, J. Lee, L. Chernyak, J. Yang, F. Ren, S.J. Pearton, S. Khodorov, and I. Lubomirsky, AIP Adv. **9**, 015127 (2019).
8. E.B. Yakimov, A.Y. Polyakov, N.B. Smirnov, I.V. Shchemerov, J. Yang, F. Ren, G. Yang, J. Kim, and S.J. Pearton, J. Appl. Phys. **123**, (2018).
9. J. Lee, E. Flitsiyan, L. Chernyak, J. Yang, F. Ren, S.J. Pearton, B. Meyler, and Y.J. Salzman, Appl. Phys. Lett. **112**, 5 (2018).
10. J.B. Varley, A. Janotti, C. Franchini, and C.G. Van de Walle, Phys. Rev. B **85**, 4 (2012).
11. A.Y. Polyakov, N.B. Smirnov, I.V. Shchemerov, S.J. Pearton, F. Ren, A.V. Chernykh, P.B. Lagov, and T.V. Kulevoy, APL Mater. **6**, 096102 (2018).
12. S. Marcinkevičius and J.S. Speck, Appl. Phys. Lett. **116**, 132101 (2020).
13. S. Yamaoka, Y. Furukawa, and M. Nakayama, Phys. Rev. B **95**, 094304 (2017).

14. O. Koksal, N. Tanen, D. Jena, H. Xing, and F. Rana, Appl. Phys. Lett. **113**, 252102 (2018).

15. J. Yang, C. Fares, Y. Guan, F. Ren, S.J. Pearton, J. Bae, J. Kim, and A. Kuramata, J. Vac. Sci. Technol. B **36**, 031205 (2018).

16. J. Yang, Z. Chen, F. Ren, S.J. Pearton, G. Yang, J. Kim, J. Lee, E. Flitsiyan, L. Chernyak, and A. Kuramata, J. Vac. Sci. Technol. B Nanotechnol. Microelectron. **36**, (2018).

17. H.J. Leamy, J. Appl. Phys. **53**, R51-R80 (1982).

18. K.L. Luke, O.v. Roos, and L.j. Cheng, J. Appl. Phys. **57**, 1978-1984 (1985).

19. C.A. Dimitriadis, J. Phys. D: Appl. Phys. **14**, 2269-2274 (1981).

20. L. Chernyak, A. Osinsky, H. Temkin, J.W. Yang, Q. Chen, and M. Asif Khan, Appl. Phys. Lett. **69**, 2531-2533 (1996).

21. S. Modak, L. Chernyak, M.H. Xian, F. Ren, S.J. Pearton, S. Khodorov, I. Lubomirsky, A. Ruzin, and Z. Dashevsky, J. Appl. Phys. **128**, 085702 (2020).

22. S. Modak, L. Chernyak, S. Khodorov, I. Lubomirsky, A. Ruzin, M. Xian, F. Ren, and S.J. Pearton, ECS J. Solid State Sci. Technol. **9**, 045018 (2020).

23. S. Modak, L. Chernyak, S. Khodorov, I. Lubomirsky, J. Yang, F. Ren, and S.J. Pearton, ECS J. Solid State Sci. Technol. **8**, Q3050-Q3053 (2019).

24. J. Lee, E. Flitsiyan, L. Chernyak, S. Ahn, F. Ren, L. Yuna, S.J. Pearton, J. Kim, B. Meyler, and J. Salzman, ECS J. Solid State Sci. Technol. **6**, Q3049-Q3051 (2016).

25. O. Lopatiuk-Tirpak, L. Chernyak, F.X. Xiu, J.L. Liu, S. Jang, F. Ren, S.J. Pearton, K. Gartsman, Y. Feldman, A. Osinsky, and P. Chow, J. Appl. Phys. **100**, 086101 (2006).

26. O. Lopatiuk-Tirpak, L. Chernyak, L.J. Mandalapu, Z. Yang, J.L. Liu, K. Gartsman, Y. Feldman, and Z. Dashevsky, Appl. Phys. Lett. **89**, 142114 (2006).

27. L. Chernyak, A. Schulte, A. Osinsky, J. Graff, and E.F. Schubert, Appl. Phys. Lett. **80**, 926-928 (2002).

28. L. Chernyak, G. Nootz, and A. Osinsky, Electron. Lett. **37**, 922-923 (2001).

29. M. Eckstein and H.U. Habermeier, J. Phys. IV **01**, C6-23-C6-28 (1991).

30. T. Onuma, S. Fujioka, T. Yamaguchi, M. Higashiwaki, K. Sasaki, T. Masui, and T. Honda, Appl. Phys. Lett. **103**, 3 (2013).

31. L. Binet, and D. Gourier, *Origin of the blue luminescence of β-Ga2O3*, in *J. Phys. Chem. Solid*, 1998. p. 1241-1248.

32. M. Maiberg, T. Hölscher, S. Zahedi-Azad, and R. Scheer, J. Appl. Phys. **118**, 105701 (2015).

33. T. Onuma, Y. Nakata, K. Sasaki, T. Masui, T. Yamaguchi, T. Honda, A. Kuramata, S. Yamakoshi, and M. Higashiwaki, J. Appl. Phys. **124**, 075103 (2018).

34. B.E. Kananen, N.C. Giles, L.E. Halliburton, G.K. Foundos, K.B. Chang, and K.T. Stevens, J. Appl. Phys. **122**, 6 (2017).

35. T.T. Huynh, L.L.C. Lem, A. Kuramata, M.R. Phillips, and C. Ton-That, Phys. Rev. Mater. **2**, 105203 (2018).

36. M. Maiberg and R. Scheer, J. Appl. Phys. **116**, 123711 (2014).

37. M. Maiberg and R. Scheer, J. Appl. Phys. **116**, 123710 (2014).

38. E. Chikoidze, A. Fellous, A. Perez-Tomas, G. Sauthier, T. Tchelidze, C. Ton-That, T.T. Huynh, M. Phillips, S. Russell, M. Jennings, B. Berini, F. Jomard, and Y. Dumont, Mater. Today Phys. **3**, 118-126 (2017).

Figure Captions

Figure 1:(a) A schematic diagram of the sample structure and experimental setup. **(b)** An example of the acquired EBIC line-scan from the control structure at 77 K. **Inset** shows the raw data with $x^{0.5}exp(-x/L)$ fit for extraction of the diffusion length.

Figure 2: Temperature dependence of diffusion length for control, alpha- and proton-irradiated structures.

Figure 3: A TRCL streak acquired at 295 K for control structure and the associated raw streak image (inset).

Figure 4: Dependence of excess carrier lifetime on temperature for control, alpha- and proton-irradiated structures.

Figure 5: Mobility calculated with Eq. (4) from independently measured L and τ for control, alpha- and proton-irradiated structures.

Figure 1

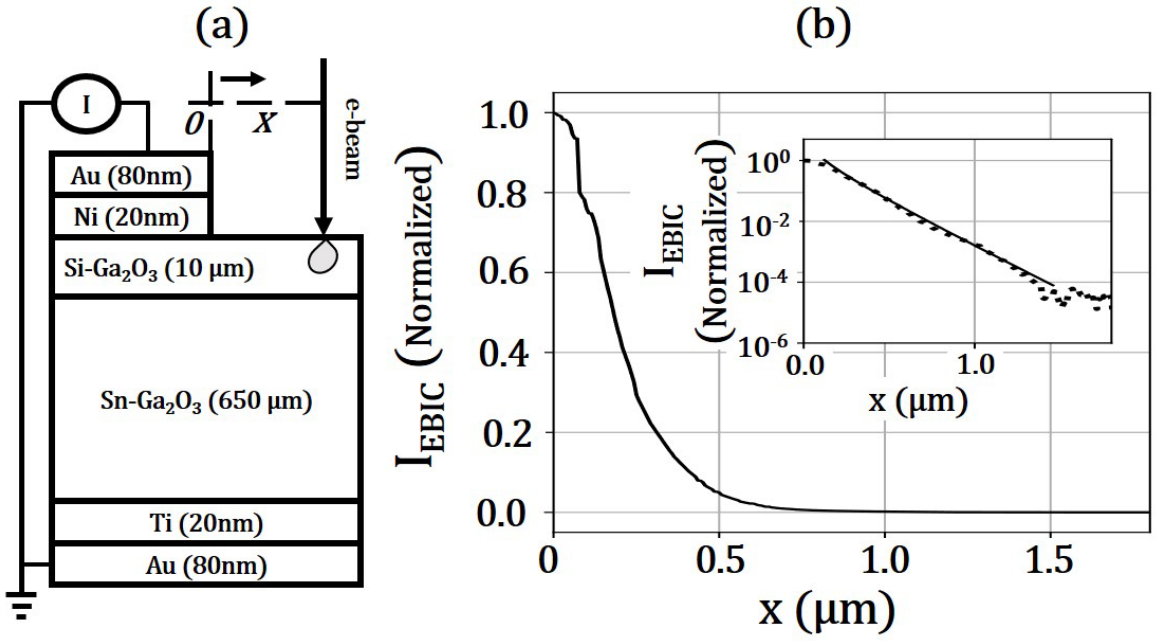
(a)
I
0
x
e-beam
Au (80nm)
Ni (20nm)
Si-Ga2O3 (10 µm)
Sn-Ga2O3 (650 µm)
Ti (20nm)
Au (80nm)
(b)
IEBIC (Normalized)
1.0
0.8
0.6
0.4
0.2
0.0
0
0.5
1.0
1.5
x (µm)
IEBIC (Normalized)
10^0
10^-2
10^-4
10^-6
0.0
1.0
x (µm)

Figure 2

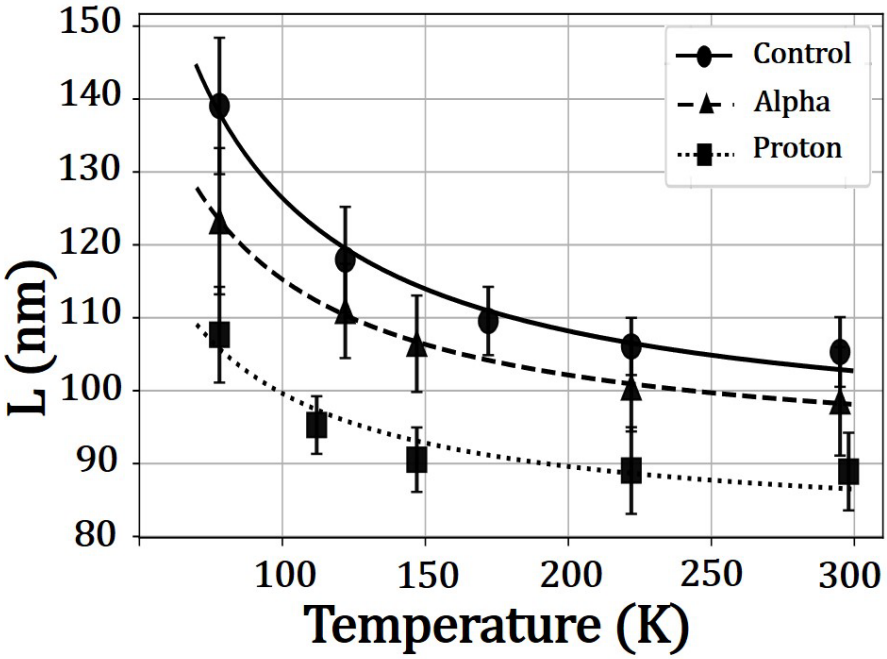
150
140
130
120
110
100
90
80
L (nm)
100
150
200
250
300
Temperature (K)
Control
Alpha
Proton

Figure 3

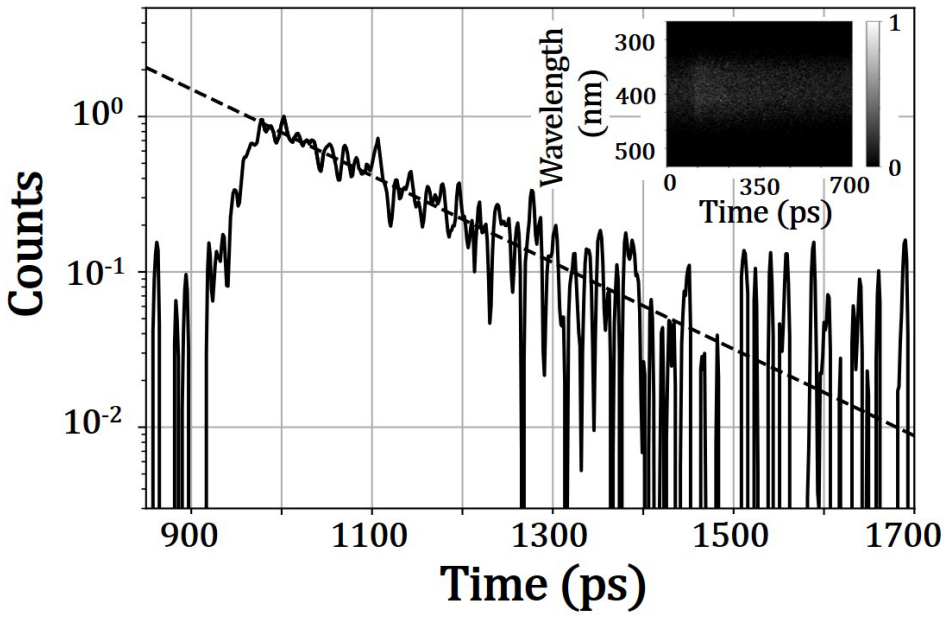
Counts
10^0
10^{-1}
10^{-2}
900
1100
1300
1500
1700
Time (ps)
Wavelength (nm)
300
400
500
0
350
700
Time (ps)
1
0

Figure 4

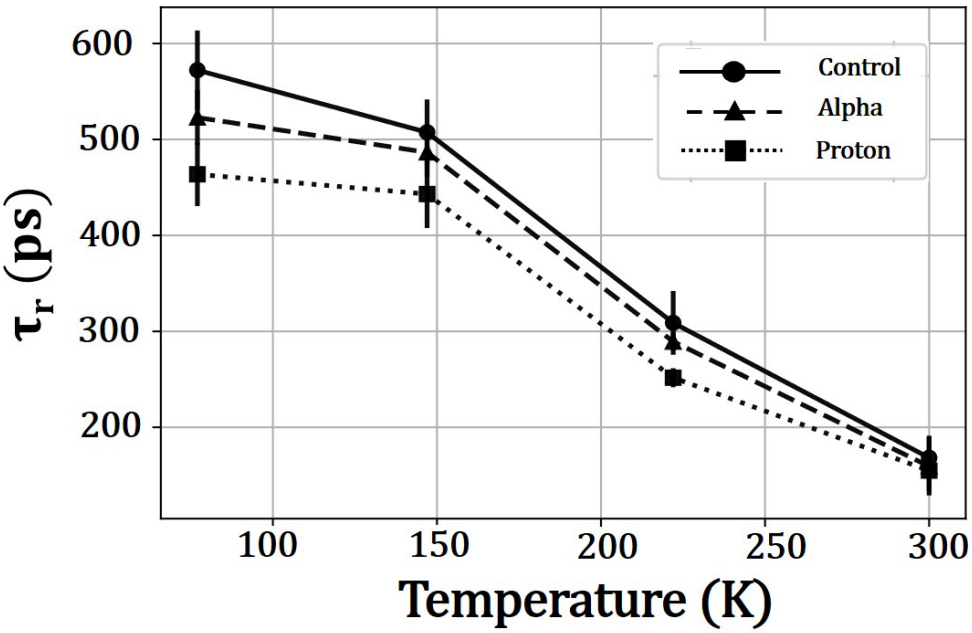
600
500
400
300
200
τ_r (ps)
100
150
200
250
300
Temperature (K)
Control
Alpha
Proton

Figure 5

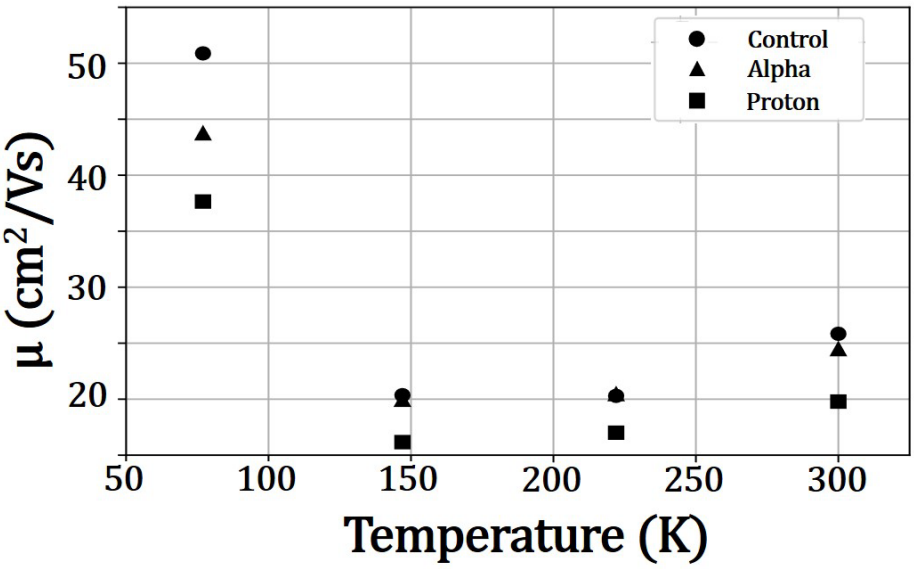
Control
Alpha
Proton
μ (cm²/Vs)
50
40
30
20
50
100
150
200
250
300
Temperature (K)